



HAL
open science

Numerical investigation of several twisted tubes with non-conventional tube cross sections on heat transfer and pressure drop

Bruce Indurain y Urricelqui, David Uystepuyst, François Beaubert, Sylvain Lalot, Asdis Helgadottir

► **To cite this version:**

Bruce Indurain y Urricelqui, David Uystepuyst, François Beaubert, Sylvain Lalot, Asdis Helgadottir. Numerical investigation of several twisted tubes with non-conventional tube cross sections on heat transfer and pressure drop. *Journal of Thermal Analysis and Calorimetry*, 2020, 140 (3), pp.1555-1568. 10.1007/s10973-019-08965-4 . hal-03545598

HAL Id: hal-03545598

<https://uphf.hal.science/hal-03545598v1>

Submitted on 27 Jan 2022

HAL is a multi-disciplinary open access archive for the deposit and dissemination of scientific research documents, whether they are published or not. The documents may come from teaching and research institutions in France or abroad, or from public or private research centers.

L'archive ouverte pluridisciplinaire **HAL**, est destinée au dépôt et à la diffusion de documents scientifiques de niveau recherche, publiés ou non, émanant des établissements d'enseignement et de recherche français ou étrangers, des laboratoires publics ou privés.

NUMERICAL INVESTIGATION OF SEVERAL TWISTED TUBES WITH NON-CONVENTIONAL TUBE CROSS-SECTIONS ON HEAT TRANSFER AND PRESSURE DROP

*B. Indurain¹, D. Uystepuyst¹, F. Beaubert¹, S. Lalot¹ and Á. Helgadóttir²

¹ LAMIH UMR CNRS 8201, Polytechnic University Hauts-de-France, 59300, Valenciennes, France.
bruce.indurainyurricelqui@uphf.fr (corresponding author)

² Faculty of Industrial Engineering, Mechanical Engineering and Computer Science, University of Iceland,
Hjardarhagi 2-6, 107 Reykjavik, Iceland

ABSTRACT

Numerical simulations were performed with the open-source CFD software OpenFOAM to investigate the ability of several configurations of short length twisted tube geometries with non-circular cross-section connected to tubes with circular cross-section to induce a swirling flow. The heat transfer and the pressure drop linked to the generated swirling flow are also calculated. The swirling flow is modeled using a $k-\omega$ SST turbulence model with a Low-Reynolds approach. It is shown that a short length twisted tube with an elliptical cross-section (STE) is able to generate a swirling flow but its intensity greatly depends on its twist pitch and its aspect ratio. The lower the aspect ratio, the higher the swirl intensity. For a Reynolds number ranging from 10 000 to 100 000, the results reveal that compared to a plain tube, the STE with the lowest aspect ratio achieves to enhance the heat transfer from 22 to 90 % at the cost of an increased pressure drop of respectively 63 and 129 %. The second part of the study is focused on a short length twisted tube with a three-lobed cross-section (ST3L) and the results reveal that the generated swirling flow is even more intense than with the STE and that the heat transfer enhancement goes from 30 to 105 % at the cost of an increased pressure drop from 137 to 180 %.

ARTICLE HIGHLIGHTS

- Elliptical and three-lobed cross sections twisted tube can generate long lasting swirling decaying flows.
- The decay rate of the swirling flow remains approximatively the same for all the studied geometries.
- The Performance Enhancement Coefficient of all investigated geometries are similar and are close or above 1.

KEYWORDS

Twisted tubes; Elliptical; Three-lobed; Decaying swirling flow; Heat transfer; CFD.

Nomenclature

a major axis of the ellipse, m
A wetted area, m²
b minor axis of the ellipse, m
c aspect ratio of the ellipse, dimensionless
c_p specific heat capacity, J.kg⁻¹.K⁻¹
C_f skin friction coefficient, dimensionless
Δp pressure drop, Pa
D_h hydraulic diameter, m
e quantity to evaluate for the GCI
f friction factor coefficient, dimensionless
GCI Grid Convergence Index

h heat transfer coefficient, W.m⁻².K⁻¹
I turbulence intensity, dimensionless
k turbulent kinetic energy, J.kg⁻¹
l turbulent mixing length, m
L total length of the tested tube, m
m mass flow rate, kg.s⁻¹
Nu Nusselt number, dimensionless
P twist pitch, m
r refinement ratio, dimensionless
Re Reynolds number, dimensionless
S Swirl number, dimensionless
T temperature, K
U fluid velocity, m.s⁻¹

Q	heat flux, W
z	axial position, m
z*	dimensionless axial position ($z.D_h^{-1}$)
z ₁ *	downstream dimensionless axial position z^*-24
α	order of accuracy for the GCI, dimensionless
λ	thermal conductivity, $W.m^{-1}.K^{-1}$
μ	dynamic viscosity, Pa.s
ρ	fluid density, $kg.m^{-3}$
τ_w	wall shear stress, Pa
ω	turbulent kinetic energy dissipation rate, s^{-1}

Subscript

0	<i>inlet value</i>
b	bulk
down	downstream tube
LMTD	Logarithmic Mean Temperature Difference
in	inlet of energy balance ($z^*=0$)
out	outlet of energy balance ($z^*=51$)
p	plain tube
STE	short element of twisted oval tube
ST3L	short element of twisted three-lobed tube
tr	transition tube
up	upstream tube
w	wall

Superscripts

–	area averaged quantity
---	------------------------

INTRODUCTION

Increasing the heat transfer at the wall of a tube is particularly challenging when the pressure drop has to be maintained at a low level and this is specifically the aim of the present study. The typical solution is to introduce a twisted tape; see e.g. [1] for a quite recent review. Bahiraei et al. numerically studied the effect of several twisted tapes arrangements combined with nanofluids and their results showed that using twin counter twisted tapes improves the heat transfer rate with minimum energy consumption because this twisted tapes configuration generates a more intense swirling flow and reduce total entropy generation compared to a single twisted tape or twin co-twisted tapes [2,3]. But the pressure drop increase is often too high even with self-rotating twisted tapes [4]. Some authors have suggested to cut the continuous tape and studied the influence of the separating distance between these regularly spaced twisted tapes; see e.g. [5]. It has also been suggested to use short length twisted tapes to further decrease the pressure drop; see e.g. [6]. Improvements to these short twisted tapes have been suggested in the shape of turbine blades; see e.g. [7] for a review. Another standard solution is to use internally finned tubes; see e.g. [8] for a review dealing with laminar flows and [9] for an example dealing with a turbulent flow.

As another example, Van Goethem et al. [10] numerically studied heat transfer and pressure drop

of air flow in several heat transfer enhancers and among them there were straight and helical internally finned tubes. For Reynolds numbers from 80 000 to 350 000, they reported that these increased surface technologies respectively enable an average enhancement in heat transfer of 51 % and 66 % compared to a plain tube yet at the expense of an average increased pressure drop of 67 % and 92 %.

In all cases, the better heat transfer performance is linked to the presence of a swirling flow which is characterized by both an axial and a tangential velocity component. This latest enables an intense secondary flow which disrupts the boundary layer and leads to reduce the thermal gradient between the fluid and the wall. Furthermore, swirling flows improve the mixing of the core and near wall flow which allows a more effective and homogeneous heating of the fluid flowing in the tube.

Axial guide vanes swirlers are often used to generate swirling flows with great intensity. Rocha et al. [11] have investigated the performances of an axial guide vane swirler in the laminar flow regime. They observed that, although a strong swirling flow was created, recirculations of the flow were also caused by the swirlers vanes. As a consequence the pressure drop was increased from 450 to 1000 % compared to a plain tube within the range the investigated Reynolds numbers. Another design of propeller type swirl generator was investigated by Ahmadvand et al. [12]. Their device was mounted on a central shaft and they conducted both experimental and CFD simulations to study the thermo-hydraulic performances of their swirler in the turbulent flow regime. Their results showed that their axial guide vane swirler can generate an intense swirling flow leading to an enhancement of heat transfer of 110 %. However, this is at the cost of an even greater pressure drop and their CFD results revealed that this drawback is mainly caused by the geometry of the swirler itself. Experimental results from Bali and Sarac [13] on the effect of one or two axial guide vanes swirler placed in series on heat transfer and pressure drop proved that swirling flows and more specifically decaying swirling flows can greatly enhance heat transfer. However their results also pointed out that axial guide vanes swirler are generating too much pressure drop and in turn this kind of device could be detrimental for some applications.

A less conventional solution is to use "deformed" cross-sections that are twisted along the tube axis. For example, tubes with elliptical cross-sections have been studied and some of those researches focused on the heat transfer and pressure drop performances of twisted elliptical tube either in the laminar flow regime [14] or in the turbulent flow regime [15, 16]. They all concluded to a heat

transfer enhancement at a reasonable pressure drop penalty compared to the previously mentioned passive techniques. Tan et al. [17] conducted a parametric study of a twisted elliptical tube and they reported that this kind of tube geometry offers an excellent improvement of the heat transfer compared to the increased pressure loss. It can also be concluded from their study that the greater the aspect ratio of the ellipse the higher the benefit and this is also true with the twist pitch of the tube but up to a given value. This latest result shows that continuous swirling flow can become less efficient if it is maintained over a too long distance. Thus, after reaching a fully developed state, the swirling flow should decay not to increase pressure drop further.

Yet, another possibility is to use lobed cross-sections as presented in [18-19]. Jafari et al. [20] studied experimentally and numerically the thermo-hydraulic performances of a decaying swirling flow generated by a three-lobed tube and they showed that this kind of swirler offers a good compromise between heat transfer enhancement and increased pressure drop. Zhou et al. [21] numerically studied a similar three-lobe tube along with an internal spiral vanes and a rifle tube and they showed that the first configuration enables to reach the strongest swirling flow.

The novelty of the study is to consider short length twisted tubes instead of full length twisted tubes as studied up to now. This paper presents results of a numerical investigation using OpenFOAM on the heat transfer and pressure drop performance of a developing swirling flow generated by a short length twisted tube with elliptical cross-section (STE) and by a short length twisted tube with a three-lobed cross section (ST3L). For both cases, the fluid downstream of the short length twisted tube flows in a tube with a circular cross-section and the decay mechanism of the swirling flow for both technologies is also investigated along with its effect on pressure drop and heat transfer.

2. Non-conventional Tubes cross-sections

The most basic deformation of a circular cross section is an elliptical cross-section as illustrated in Figure 1a. The ellipse could be defined by its aspect ratio c as:

$$c = \frac{b}{a} \quad (1)$$

where, b is the minor axis and a is the major axis of the ellipse. The tube with a circular cross-section and the portion of tube with an

elliptic cross-section have the same hydraulic diameter D_h .

A more advanced cross-section could be elaborated using three circular lobes connected to each other by small arcs of circle such as presented in Figure 1b. This three-lobed cross-section could also be defined by its aspect ratio but here a and b are respectively the radius of the circumscribed and inscribed circle of the lobed cross-section. Furthermore, the depth of the arc of circle, d , is defined as the difference between the radius of the circle which supports the end points of the arc of circle and b . Finally, the width of the arc of circle is defined by the angle θ between the two end points of the arc of circle. The tube with a circular cross-section and the portion of tube with a three-lobes cross-section do not have the same hydraulic diameter D_h but the radius of the circumscribed circle a is equal to $D_h/2$.

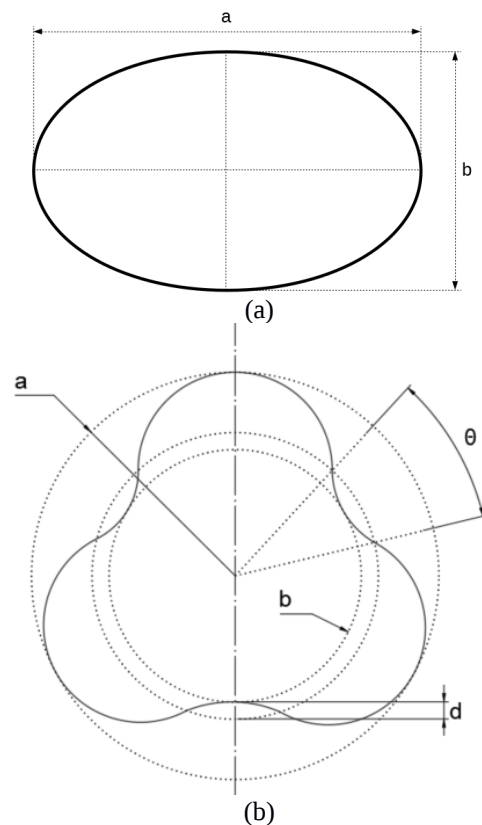
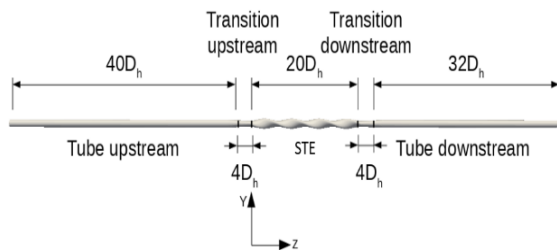


Fig.1: (a) sketch of an elliptical cross-section, (b) sketch of a three-lobed cross-section.

Revolving both those cross-sections along the tube axis yields a twisted tube. The flow inside those tubes acquires a tangential velocity component which leads to a swirling flow. However, once the swirling flow is developed the increase of wall shear stress also generates more pressure drop. Therefore, to avoid too much energetic loss, the twisted tube must only represent a small portion of the whole length of the tube in order to let the intensity of the swirling flow decay.

1 A numerical test bench was created to simulate
 2 the flow inside the twisted tube and the decay of
 3 the swirl intensity in a downstream tube with a
 4 circular cross-section. This test bench can be seen
 5 on Figure 2 and its composition is described
 6 hereafter. The diameter of the circular
 7 cross-sections tubes is $D=0.02$ m and the whole
 8 length of the test bench is $L=100 D$. The length of
 9 the twisted tube is $L_{\text{twist}}=20 D$ and its inlet is
 10 considered as the origin of the axis of coordinates
 11 ($z^*=0$). Upstream there is a tube with a circular
 12 cross-section whose length is $L_{\text{up}}=40 D$ in order to
 13 have a fully developed flow at the inlet of the
 14 twisted tube. Downstream of the twisted tube, there
 15 is another tube with a circular cross-section where
 16 the swirling flow decays and with a length
 17 $L_{\text{down}}=32 D$. To ensure the continuity between the
 18 twisted tube and upstream and downstream tubes,
 19 transition elements are placed in order to gradually
 20 evolve from a circular to an elliptical or a
 21 three-lobe cross-section and vice-versa. Those
 22 transition elements have a length $L_{\text{transitions}}=4 D$.
 23 Considering the whole length of the numerical test
 24 bench, the length of the twisted tube is relatively
 25 small, that is why the twisted tube will be referred
 26 to as Short Element of Twisted Elliptical Tube
 27 (STE) if its cross-section is an ellipse or Short
 28 Element of Twisted Three-Lobed Tube (ST3L)
 29 otherwise.



30 Fig.2: Sketch of the numerical test bench with
 31 $P=10D_h$.

32 The STE and ST3L are also characterized by
 33 their twist pitch P which is the distance required to
 34 perform a 360° rotation of the initial cross-section
 35 of the twisted tube. Twist pitch of 20, 10 and 5 D
 36 were tested with the STE whose aspect ratio was
 37 $c=0.6$ and those results can be found in
 38 Indurain et al. [22]. It was shown that the highest
 39 swirl intensity and the best thermal performances
 40 were achieved with a STE whose twist pitch is
 41 $P=5 D$. However, it was also with this
 42 configuration that the pressure drop was the
 43 highest. Nevertheless, it was deemed the most
 44 interesting configuration of STE because the swirl
 45 intensity was relatively high and the swirling flow
 46 lasted over a long distance in the downstream tube
 47 with $S/S_0=0.2$ at $z^*=47.5$.

48 It is well known that to reduce the pressure
 49 drop, the aspect ratio, as defined in Equation (1),

should be increased. That is why, in the first part
 of the present study, a STE with a twist pitch of $P=5D$
 and an aspect ratio of $c=0.7$ is tested in order to
 observe the influence of this parameter on heat
 transfer and pressure drop generated by the
 swirling flow.

In a second part the selected STE will be
 compared to a ST3L with the same twist pitch and
 aspect ratio.

3. Set up of the numerical simulations

The simulations are performed using the finite
 volume method with the open source CFD software
 OpenFOAM 4.1. OpenFOAM is an open source
 object oriented numerical simulation toolkit
 developed in C++ and released under GPL license
 by the OpenFOAM®Foundation [23]. No
 experimental data are available with the studied
 configurations of short length twisted tube on heat
 transfer and pressure drop performances. That is
 why, in order to give confidence in the results of
 the simulations, a validation procedure was
 performed. Tang et al. [24] conducted both an
 experimental and a numerical study on the thermal
 and energetic performances of the swirling flow
 created in a full length elliptic twisted tube and a
 full length three-lobed twisted tube as shown in
 Figure 3. Hence, once developed, the intensity of
 the swirling flow remains constant.

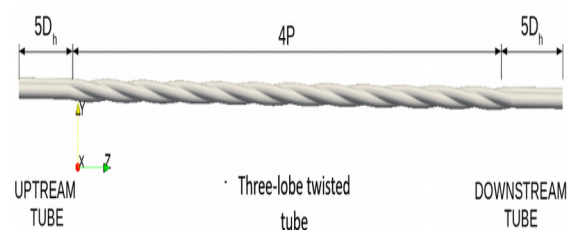


Fig.3: Reproduction of the numerical test bench
 with a three-lobed twisted tube from
 Tang et al. [24]

The cases studied by Tang et al. are
 sufficiently close to the one investigated here to be
 confident in the adopted numerical procedure once
 their results were correctly reproduced. Therefore,
 some of their numerical work was recreated and it
 is detailed in the next paragraph.

3.1 Validation procedure steps with the work of Tang et al. [24]

The first validation step is with the twisted
 tube with an elliptical cross-section. This part of
 the validation is described in Indurain et al. [22]

The second validation step is with the twisted
 tube with a three-lobed cross-section. The radii of
 the circumscribed and inscribed circle are

respectively $a=0.0105$ m and $b=0.0075$ m and the depth of the arc of circle is $d=0.0025$ m. The numerical test bench based on the work of Tang can be seen on Figure 3. It is composed of a twisted tube and two straight tubes which are located at both end of the twisted tube all having a three-lobed cross-section. The hydraulic diameter of the tube is given by Tang et al. to be $D_h=0.02$ m, the twist pitch is $P=10D_h$ and the length of the twisted tube is $L_{TANG}=4P$.

3.2. Boundary conditions and numerical schemes

In the numerical simulation of Tang et al. the working fluid is water whose thermodynamic properties are presented in table 1 and the conditions regarding the flow are: steady state, incompressible, turbulent with heat transfer. Several boundary conditions are imposed. Among them, at the inlet a flat velocity profile is given with the magnitude of the bulk velocity which is calculated based on the Reynolds number. At the inlet, the flow has a constant temperature of $T_0=300$ K and a zero normal gradient for the pressure. All along the $100D$ of the numerical test bench, at the wall of the tubes a constant temperature $T_w=350$ K and a no-slip velocity condition are applied. At the exit of the computational domain, a constant pressure is imposed while the normal spatial gradient of the velocities and the temperature are equal to zero.

Table 1. Thermodynamic properties of the fluid (water) used for the validation case from Tang et al. [24].

c_p	4175
λ	0.6472
μ	0.549e-3
ρ	998.2

The simulations run until the residuals for the continuity and momentum equations are below 10^{-6} and 10^{-9} for the energy equation. Probes also monitored the evolution of the pressure and the temperature at the tubes axis and close to the wall at different axial locations inside the twisted tube and in the tube downstream. The simulations were deemed to have reached a numerical steady state when the monitored quantities did not change for more than 5,000 iterations. In order to save time, the simulations were parallelized on 32 processors using OpenFOAM MPI.

All components of the continuity, momentum and energy equations are discretized using a second order bounded linear UPWIND scheme. The pressure-velocity linked equations are solved using the SIMPLE algorithm. In the work of Tang et al. a turbulence model sensitivity study shows that the

k - ω SST turbulence model with standard wall functions give the results with the lowest deviation from the experimental data and is therefore adopted. Nonetheless, accurate simulations of swirling flows greatly depend on how the variables of the flow are calculated in the boundary layer, thus in order to compute more accurately both the dynamic and thermal boundary layers a Low-Re approach is used instead of using standard wall functions to reproduce the numerical work of Tang et al. At the inlet, the value of the turbulent kinetic energy k and the turbulent dissipation frequency ω are set using the equations recommended by Robertson et al. [25]:

$$k = \frac{3}{2} (U_0 I)^2 \quad (2)$$

where,

$$I = 0.16 Re^{-\frac{1}{8}} \quad (3)$$

and

$$\omega = \frac{\sqrt{k}}{l} \quad (4)$$

where l is the turbulent mixing length defined as:

$$l = 0.07 D_h \quad (5)$$

At the outlet, a null flux boundary condition is imposed for both turbulent quantities and fixed values are imposed at the wall. The latter are 10^{-10} for k and 10^6 for ω .

3.3. Validation of the numerical procedure

The friction factor is used to determine the energetic losses caused by the pressure drop between the inlet and outlet of the twisted tube and is calculated as:

$$f = 2 \frac{\Delta p D_h}{\rho U_b^2 L} \quad (6)$$

The Nusselt number, Nu , is used to determine the amount of heat transported by the swirling flow and is defined as:

$$Nu = \frac{h D_h}{\lambda} \quad (7)$$

The heat transfer coefficient h is calculated by using an energy balance between the heat transferred from the wall of the tube to the fluid:

$$\dot{Q} = \pi D_h L h T_{LMTD} \quad (8)$$

where:

$$T_{LMTD} = \frac{\bar{T}_{out} - \bar{T}_{in}}{\ln \left(\frac{T_w - \bar{T}_{out}}{T_w - \bar{T}_{in}} \right)} \quad (9)$$

and the energy absorbed by the fluid between two positions inside the tube:

$$\dot{Q} = \dot{m} c_p (\bar{T}_{out} - \bar{T}_{in}) \quad (10)$$

The convective heat transfer coefficient is derived from Equation (8) and (10) and it is then easy to calculate the Nusselt number from Equation (7):

$$Nu = \frac{\dot{m} c_p (\bar{T}_{out} - \bar{T}_{in})}{\pi \lambda L T_{LMTD}} \quad (11)$$

The mean values of the temperatures T_{out} and T_{in} are calculated by using the bulk temperature in the given cross-section and is defined as:

$$\bar{T} = \frac{1}{U_b A} \int_A T u_z dA \quad (12)$$

The results of the simulations with the twisted three-lobed tube of the present study are compared to the experimental data of Tang et al. [24] and are shown in Table 2. It can be observed that the results of the present simulations closely match the experimental data of Tang et al. for both the friction factor and the Nusselt number with a maximum relative deviation of respectively 3.0 and 5.4 %. As a consequence, the adopted numerical procedure is deemed reliable to predict the heat transfer and the pressure drop caused by a swirling flow.

Table 2. Comparison between the results from the simulations of the present study and the experimental data from Tang et al. [24].

Re	14,000	16,000	18,000	20,000
f_{Tang} [24]	0.034	0.033	0.032	0.030
f	0.033	0.032	0.031	0.0299
Rel. dev	1.7%	2.9%	3.0%	0.21%
Nu_{Tang} [24]	79.3	88.1	96.2	103.6
Nu	83.6	90.7	94.9	98.9
Rel. dev	5.4%	3.0%	1.3%	4.5%

4. Numerical simulations of the twisted tubes

The same numerical configuration (boundary conditions, numerical schemes, level of convergence of the residuals, stationarity of the monitored values) as in the validation process of part 3 is kept here. However, the working fluid is now air and the thermodynamic properties used are summed up in Table 3. One assumption is that, within the given range of encountered temperatures, the thermodynamic properties are kept constant.

Table 3. Thermodynamic properties of the fluid (air) used for the present study simulations.

c_p	1006
λ	0.04
μ	1.91e-5
ρ	1.205

Although the numerical procedure has been validated, a mesh independent test study is undertaken to ensure that the results of the simulations are not mesh sensitive.

4.1. Mesh independence test

The Grid Convergence Index (GCI) method developed by Roache [26] is adopted here to conduct the mesh independence test. It is a generalization of the Richardson extrapolation and it provides a uniform measure of convergence for grid refinement studies. The GCI value represents the resolution level and how much the solution approaches the asymptotic value and the GCI is defined as:

$$GCI_i = 1.25 \frac{e_{i+1} - e_i}{e_i (r^\alpha - 1)} \quad (13)$$

where the grid refinement ratio r in this study is $r=1.43$ and α is computed as follow [26]:

$$\alpha = \frac{\ln \left(\frac{e_1 - e_2}{e_2 - e_3} \right)}{\ln(r)} \quad (14)$$

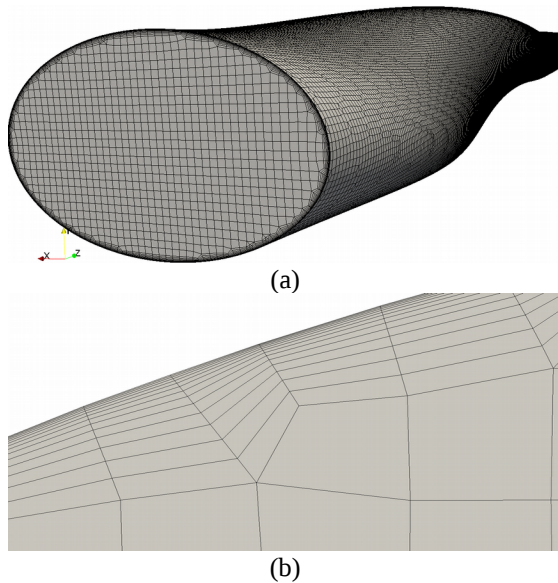
For the sake of clarity, the GCI method is not described here but can be found in [26,27]. Both global and local quantities are investigated with the GCI method. The global quantities are the friction factor f and the Nusselt number Nu . The local quantities are averaged values in a cross-section located in $z^*=34$ and they are the skin friction coefficient C_f defined as:

$$C_f = 2 \frac{\tau_w}{\rho U_b^2} \quad (15)$$

and the bulk temperature T_b defined in Equation (12).

The meshing process is achieved by using cfMesh, an open source meshing software developed by Dr. Franjo Juretic [27]. For the STE configuration, three different unstructured meshes were tested with a refined mesh close to the wall of the tube consisting in 11 additional mesh layers. The three meshes from the finest to the coarsest are noted mesh 1, mesh 2 and mesh 3 and they respectively have 10,890,272, 7,632,400 and 5,330,459 cells. The largest cell size of all the three meshes are respectively 2.75, 3.0 and 3.5 % of the

1 tube diameter. Mesh 2 is obtained with the same
 2 meshing parameters used for the validation case.
 3 Clips of the meshed geometry with mesh 2 can be
 4 seen on Figure 4 a and b.



5
6
7
8
9
10
11
12
13
14
15
16
17
18
19
20
21
22
23
24 Fig.4: (a) Clip of the meshed geometry with mesh
 25 2, (b) details of the mesh close to the wall of the
 26 tube.

27 The results of the grid refinement study are
 28 summarized in Table 4 and it can be noticed that
 29 the GCI between mesh 1 and 2 is lower than the
 30 GCI between mesh 2 and 3 except for the Nusselt
 31 number but the GCI is still low. Therefore, the
 32 results of the simulations are less prone to change
 33 between mesh 1 and mesh 2. Furthermore, it is
 34 computationally less expensive to run simulations
 35 with mesh 2, thus this latest mesh was chosen to
 36 perform all the other simulations for the parametric
 37 study.

38 Table 4. Order of accuracy and Grid
 39 Convergence Index for several flow quantities and
 40 for the three meshes.

	α	GCI ₂ (%)	GCI ₁ (%)
f	7.5	3.1	0.21
Nu	2.4	0.28	1.1
C _f	2.95	1.44	0.5
T _b	2.6	0.35	0.14

42 4.2. Low-Reynolds approach

43 As a Low-Reynolds approach is adopted in the
 44 current study for both the STE and the ST3L, the
 45 mesh close to the wall has to be sufficiently refined
 46 to guarantee $y^+ \approx 1$. The same meshing parameters
 47 were taken to mesh both the STE and the ST3L but
 48 this latest geometry is a little bit more complex
 49 than the former and thus is composed by more
 50 cells. The results of the simulations show that even
 51 under the highest Reynolds number taken for this

study ($Re=100\ 000$), the condition of $y^+ \approx 1$ is
 respected as can be seen on Table 5.

Table 5. Number of cells of the different studied
 geometries and their corresponding y^+ under
 $Re=100\ 000$.

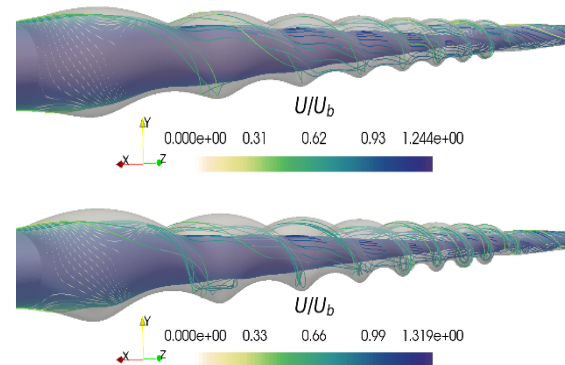
	STE	ST3L
Number of cells	7,632,400	10,656,511
mean y^+	0.62	1.01
max y^+	1.18	1.94

5. Results and discussion

5.1. Influence of the aspect ratio with the STE

5.1.1. Intensity of the swirling flow

The STE with a twist pitch $P=5D$ enables to
 have the most intense swirling flow but with the
 highest pressure drop. Thus, to reduce this
 energetic penalty the aspect ratio of the ellipse is
 increased from $c=0.6$ to $c=0.7$. As with this latest
 aspect ratio the elliptical cross-section is closer to a
 circular one the flow inside the STE should be less
 constrained. The effect of the aspect ratio for the
 same twist pitch of $P=5D$ on the swirling flow can
 be seen on Figure 5. For both cases, as the fluid
 flows inside the STE, more and more streamlines
 of the core flow go to the circumference of the
 twisted tube and in the downstream tube the flow is
 clearly turbulent and in a rotation motion.
 However, this effect is less emphasized with the
 $c=0.7$.



41
42
43
44
45
46
47
48
49
50
51
52
53
54
55
56
57
58
59
60
61
62
63
64
65
Fig.5: Swirling flow in the different STE with
 $P=5D$. Aspect ratio $c=0.6$ (top), aspect ratio
 $c=0.7$ (bottom) at $Re=10\ 000$.

To quantify the axial flux of axial velocity
 momentum converted into axial flux of tangential
 velocity momentum, a dimensionless number is
 usually used and is defined by Kitoh [28] as the
 swirl number S:

$$S = \frac{\int_0^R r^2 u_\theta u_z dr}{R \int_0^R r u_z^2 dr} \quad (16)$$

The evolution of the intensity of the swirl for the two cases and from $z^*=0$ to $z^*=51$ at the lowest Reynolds number $Re=10\ 000$ is shown on Figure 6, where the vertical bars delimits the different phase of the swirling flow as discussed hereafter. Phase 1, from $z^*=0$ to $z^*=20$, the generation and development of the swirling flow. Phase 2 at $z^*=20$ the geometrical transition between the elliptical cross-section of the STE and the circular cross-section of the downstream tube where the intensity of the swirling flow falls dramatically because of the sudden stop of the tubes rotation. And finally phase 3, from $z^*=24$ to $z^*=51$, where the intensity of the swirling flow continuously decreases until the exit of the computational domain.

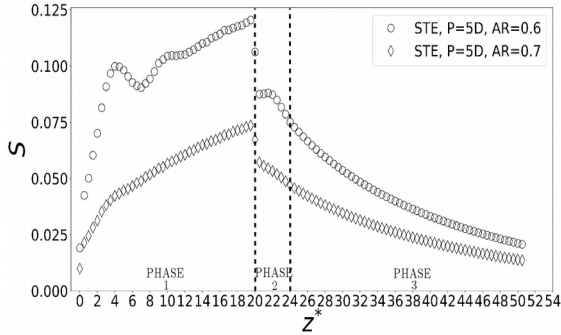


Fig.6: Evolution of the swirl number along the STE with $c=0.6$ and $c=0.7$ and downstream at $Re=10\ 000$.

It can be noticed that between the two investigated cases there are large differences in the evolution of S along the STE and downstream, especially in phase 1. While the intensity of the swirling flow increases more rapidly with $c=0.6$, it is also surprising to observe that after a rotation of 180° of the STE, S suddenly decreases and then regains its strength and further developed at a farther position in the STE. This behavior is not observed with the other case where $c=0.7$ and where the development of the swirling flow only has two phases. A first one in the first pitch, where the intensity of the swirling flow increases rapidly and a second one after the first 5D rotation of the elliptical cross-section where the intensity of the swirling flow increases with a lower slope. The maximum of S reached by both cases is also greatly different. While the STE with $c=0.6$ achieves to reach a maximum swirl intensity of $S_{max}=0.12$, the STE with $c=0.7$ remains below 0.10 with $S_{max}=0.07$.

In phase 2, even though the drop of the swirl intensity is more pronounced with $c=0.6$ than with

$c=0.7$ its S remains higher and even reaches at the end of phase 2 the same S as at the end of phase 1 with $c=0.7$.

In many investigations [29,30,31] it is reported that the decay of the swirl intensity is expected to follow an exponential trend:

$$S = S_0 e^{-\beta \frac{z}{D}} \quad (17)$$

where S_0 is the swirl intensity at the beginning of its decay and β is the decay rate.

The fit curves with Equation (17) have been calculated and can be seen on Figure 7.

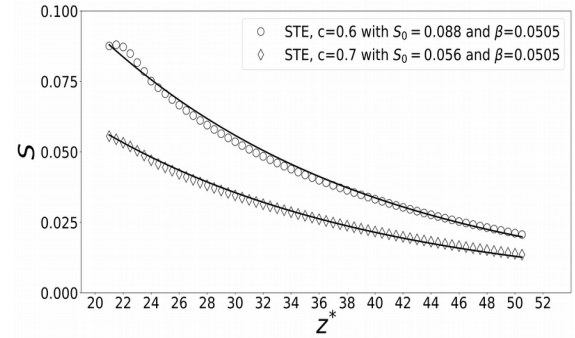


Fig.7: Evolution of the swirl intensity in STE with $c=0.6$ and $c=0.7$ and curve fitting.

The curves were fitted in the decay phase of the swirling flow. For the $c=0.6$ and $c=0.7$ cases the correlation coefficient is very good and is respectively of 0.994 and 0.996. These functions are informative because they provide the decay rate β for each swirling flow. It tends to show that the decay rate is only dependent on the Reynolds number, as shown by Beaubert et al. [32] for laminar flows, and that a kind of "fundamental flow pattern" also exists for turbulent swirling flows. As there is a good fit from the start of the swirl decay, this leads to assume that the swirling motion is close to this "fundamental" pattern from the beginning of the circular cross section:

5.1.2 Pressure drop

The swirling flow generated by the two configurations of STE are quite different from one another regarding their development in phase 1. As a consequence, the added pressure drops caused by their respective swirling flow are not the same. The pressure drop is studied by using the friction factor f as defined in Equation (6) and is computed between $z^*=0$ and $z^*=51$. The friction factor of the STE is compared to the friction factor in a plain tube, f_p which is calculated using the correlation from Pethukov:

$$f_p = \left(0.79 \ln(R_e) - 1.64\right)^{-2} \quad (18)$$

The evolution of the increase of pressure drop with the Reynolds number can be seen on Figure 8. It can be clearly seen that increasing the aspect ratio of the STE from $c=0.6$ to $c=0.7$ enables to reduce significantly the increased pressure drop. One explication could be, as the aspect ratio increases, the maximum tangential velocity reached inside the STE decreases and therefore the wall shear stress also decreases. Furthermore, with a higher aspect ratio, the curvature of the STE is less strong thus the flow can more easily follow the shape of the twisted tube. This should avoid the creation of adverse pressure gradient close to the wall leading to flow recirculation zones which causes energetic loss. The evolution of the pressure drop with the increase in Reynolds number is identical for both cases except that the STE with $c=0.7$ does not reach a plateau after $Re=80\ 000$ but keeps increasing. One of the cause of such an evolution might be the intensification of inertial forces with rotation of the fluid caused by the swirling flow. The centrifugal and Coriolis forces contribute to the energetic loss and both grow in intensity as the Reynolds number increases. Besides, this forces are proportional to the square of the velocity, hence the observed growth of f/f_p . As seen on Figure 6, the large drop of the swirl intensity in phase 2 might also be linked to high pressure drop because of the geometrical transition between the elliptical cross-section of the STE and the circular cross-section of the downstream tube in addition to the end of the rotation of the twisted tube which supports the swirling flow.

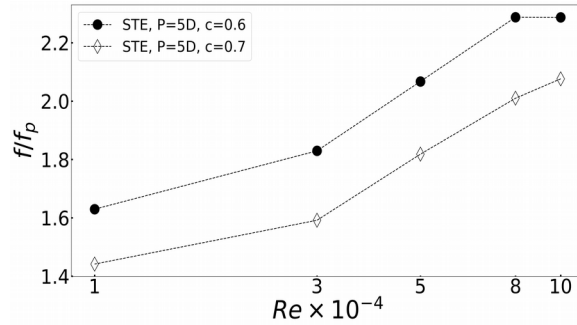


Fig.8: Evolution of f/f_p with Re for the STE with aspect ratio $c=0.6$ and $c=0.7$.

5.1.3 Heat Transfer

Along with the increase of pressure drop, the swirling flow generated by both STE also enables to enhance heat transfer between the hot wall of the tube and the cold fluid by increasing the flow path and disrupting the thermal boundary layer. The heat transfer in the STE, Nu , is calculated using Equation (11) between $z^*=0$ and $z^*=51$. The mean values of the temperature in Equation (11) are calculated using Equation (12). In a given cross-section, the temperature and the velocity at the center of each cell are used to calculate the

integral of Equation (12) using a discrete approach. The Nusselt number of the STE is compared to the heat transfer obtained in a plain tube (Nu_p) where Nu_p is calculated with the correlation of Gneilinsky:

$$Nu_p = \frac{\frac{f_p}{8}(R_e - 1000) Pr}{1 + 12.7 \left(\frac{f_p}{8}\right)^{0.5} Pr^{0.6666 - 1}} \quad (19)$$

where Pr is the Prandtl number and is defined as:

$$Pr = \frac{\mu C_p}{\lambda} \quad (20)$$

The evolution of the enhanced heat transfer with the Reynolds number can be seen on Figure 9. Although, the STE with $c=0.6$ enables a higher heat transfer enhancement than with $c=0.7$, the differences are quite small. This latest result is surprising because as seen on Figure 6, the STE with $c=0.7$ generates a swirling flow with a lower intensity than the STE with $c=0.6$. Therefore, it could have been expected that the heat transfer enhancement with STE with $c=0.7$ would have been even lower. However, even though the swirl intensity is lower with this latest STE than with STE where $c=0.6$, the level of turbulence should be greatly increased in both cases. Thus the heat transfer enhancement might also be linked to this intensified level of turbulence in the swirling flow. For instance, at $Re=100\ 000$ the maximum turbulent kinetic energy reached in STE with $c=0.6$ and $c=0.7$ is respectively 140.7 and 124.0 $J.kg^{-1}$. Besides, note that the increase in heat transfer Nu/Nu_p between $Re=10\ 000$ and $Re=100\ 000$ is greater than the increase in friction factor.

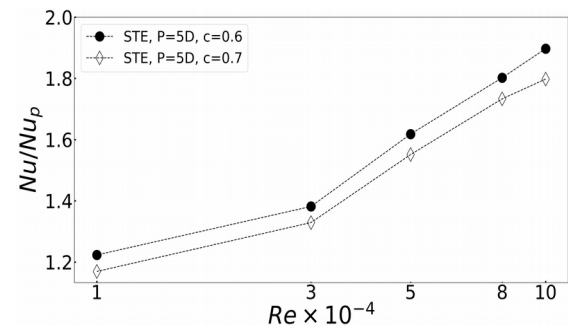


Fig.9: Evolution of Nu/Nu_p with Re for the STE with aspect ratio $c=0.6$ and $c=0.7$.

Both versions of STE can significantly enhance the heat transfer but this is at the cost of a greater pressure drop. These parameters have to be both taken into account in order to estimate the efficiency of the STE. To that end, the Performance Evaluation Criterion (PEC) proposed by Webb et al. [33] is used here and is defined as:

$$PEC = \frac{Nu/Nu_p}{\sqrt[3]{f/f_p}} \quad (21)$$

The evolution of the PEC for the different STE is shown on Figure 10. It can be observed that, the obtained PEC for both cases are similar and also always greater than 1. Only at the highest Reynolds number, the PEC of the STE with $c=0.6$ is obviously higher than the PEC of the STE with $c=0.7$. It is also interesting to note that the PEC increases with the Reynolds number indicating that there is a good balance between heat transfer enhancement and pressure drop increase. This might be due to how the swirling flow is generated which is by a continuous deformation of the tube shape. On the one hand, the flow path is extended enabling more heat exchanges between the tube wall and the fluid and the swirling flow becomes more intense which leads to a greater mixing and thus a better heat transfer. On the other hand, as the Reynolds number increases, pressure drop evolves at a lower pace and it is likely due to the absence of extended surface exchange (twisted tapes, finned tubes, axial guide vanes swirler, ect.) in the twisted tube. Despite the greater pressure drop in the STE with $c=0.6$, its better heat transfer enhancement yields a PEC which is almost the same as the STE with $c=0.7$. Nevertheless, the STE with $c=0.6$ is more interesting because it creates a more intense swirling flow which should last over a longer distance than the swirling flow created by the STE with $c=0.7$. Using Equation (17), a swirl number of 0.01 is achieved after about $34D$ for the STE with $c=0.7$, when about $43D$ are necessary for the STE with $c=0.6$.

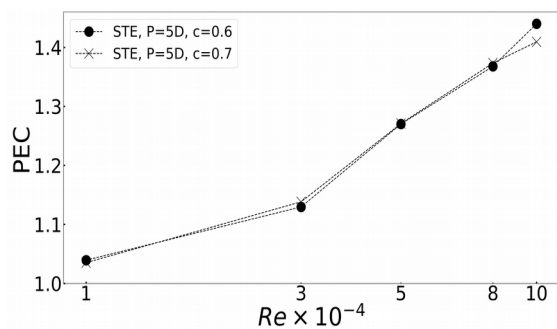


Fig.10: Evolution of the PEC with Re for the STE with aspect ratio $c=0.6$ and $c=0.7$

5.2. Influence of the cross-section: STE and ST3L

The configuration of the STE with a twist pitch of $P=5D$ and an aspect ratio of $c=0.6$ is kept and those parameters are also maintained to create the geometry of the twisted tube with a three-lobe cross-section.

5.2.1. Intensity of the swirling flow

The modification of the cross-section from an ellipse to a three-lobed enables to better divide the incoming flow from the upstream tube and to induce a swirling flow more efficiently. Figure 11 shows the distribution of the tangential velocity in a cross-section of the twisted tube at several axial positions located within the first twisted pitch at $Re=10\,000$. It can be observed that as the flow progresses in the twisted tube, an increasing fraction of the bulk velocity U_b is transformed into a rotation motion close to the wall of the tube. This fraction is notably greater in the ST3L than in the STE. This might be attributed to the fact that a dedicated portion of the flow follows a helical path inside one of the lobes of the twisted tube whereas in the STE the core flow is not divided in such a way thus it is more difficult to induce a tangential velocity to the whole flow.

The evolution of the intensity of the swirl for the two configurations of twisted tube is shown on Figure 12.

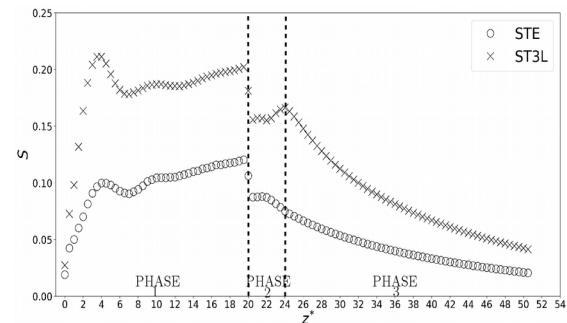


Fig.12: Evolution of the swirl number in the STE and ST3L and downstream at $Re=10\,000$.

Again, the evolution of the swirl intensity can be divided into three sections. The ST3L enables the generation of a swirling flow which is double as intense as for STE in phase 1. The development of the swirling flow in phase 1 of the ST3L is very similar to the one in the STE from $z^*=0$ to $z^*=10$. However, whereas in the STE the intensity of the swirling flow increases again after the small drop at $z^*=7$ and achieves to exceed its value at $z^*=4$, in the ST3L the peak at $z^*=3$ is not exceeded further downstream. The two tubes configurations have the same behavior at the beginning of phase 2: a tremendous drop of the swirl intensity. It could also be noted that the decrease of the swirl intensity between the end of phase 1 and the end of phase 2 is slightly higher for the STE than for the ST3L.

In phase 3, both swirling flows decay at their own pace. To further investigate the decay rate of the swirling flow from the ST3L, an exponential function from Equation (17) was fitted against the data of the swirl intensity at $Re=10\,000$. This is shown on Figure 13. It could be noted that the decay of the swirling flow for the ST3L fits quite

1
2
3
4
5
6
7
8
9
10
11
12
13
14
15
16
17
18
19
20
21
22
23
24
25
26
27
28
29
30
31
32
33
34
35
36
37
38
39
40
41
42
43
44
45
46
47
48
49
50
51
52
53
54
55
56
57
58
59
60
61
62
63
64
65

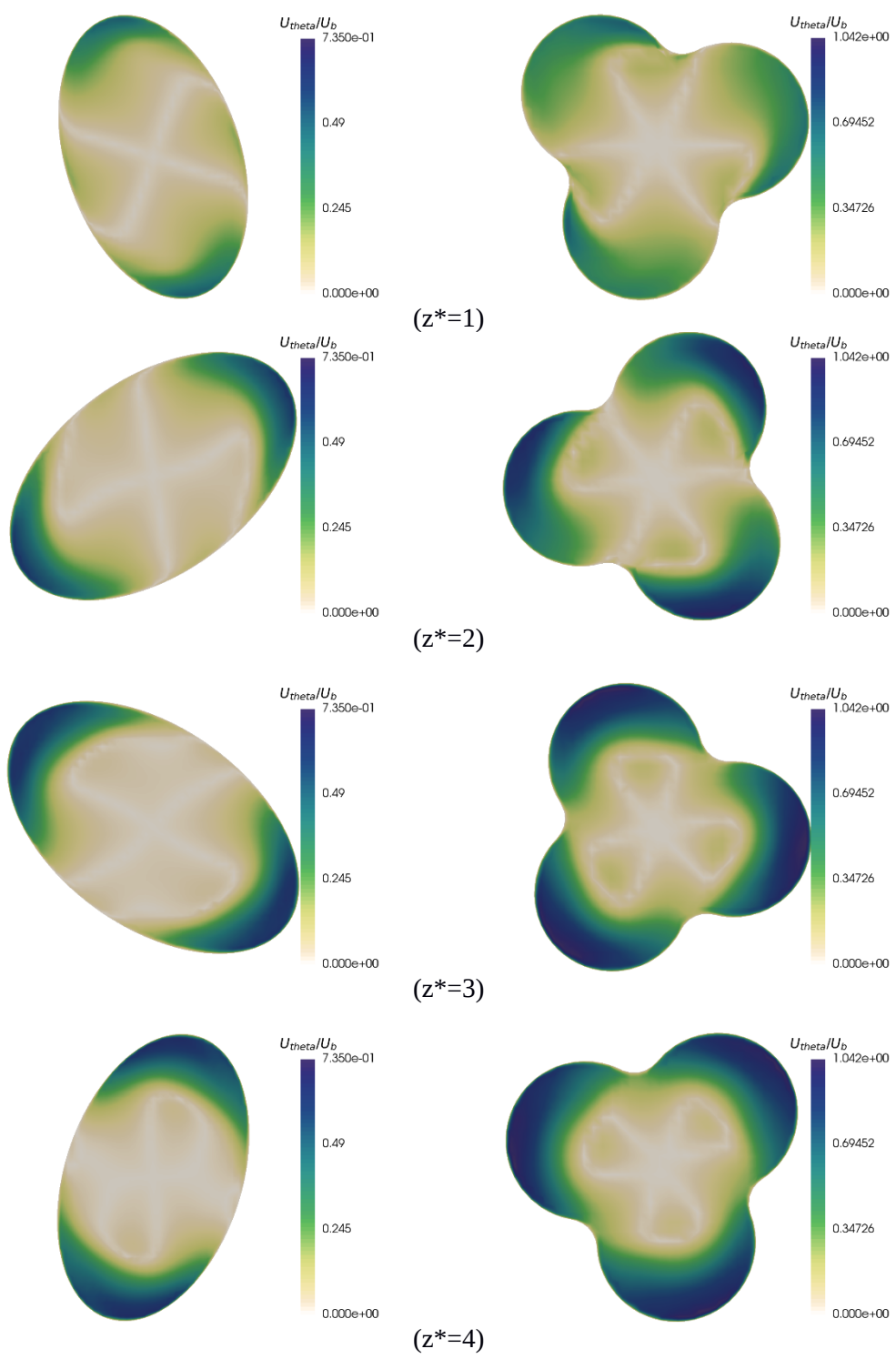


Fig.11: Axial evolution of the tangential velocity inside the first twist pitch of the STE (left) and ST3L (right).

well with the decay coefficient $\beta=0.0505$ determined for the STE if it is considered that it is shifted in space by 1.5 D, and having an initial value of $S_0=0.165$ ($S=0.165 \exp(-0.0505(z_1^*))$). The correlation coefficient is also good with $R^2=0.985$. In that case the decrease is higher in the first part of phase 3; for about 6 D. This might be due to the fact that the three-lobed section does not lead to the "fundamental" swirling flow pattern and that it is necessary to have a transition zone where the "non-fundamental" part of the flow pattern is dissipated. Note that in Beaubert et al. [32] it is shown that this transition zone represents about 4D for a complex laminar flow. It can also be concluded that the decay of the STE corresponds to the decay of the ST3L if it is shifted by 10.9D.

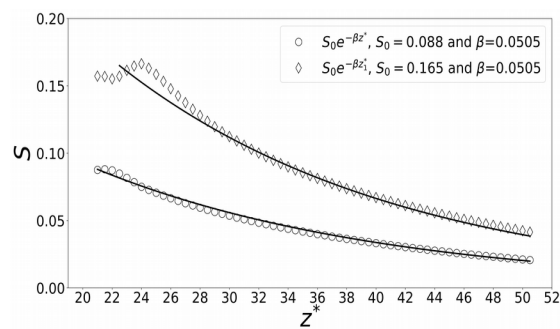


Fig. 13. Evolution of the swirl intensity downstream the STE and ST3L and curve fitting at $Re=10\ 000$.

5.2.2. Pressure drop

The evolution of the friction factor increase for the STE and the ST3L with the Reynolds number is shown on Figure 14.

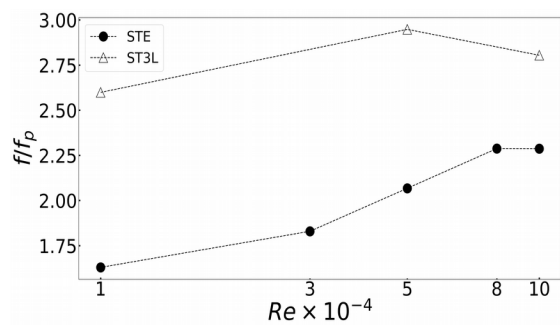


Fig.14: Evolution of f/f_p with Re for the STE and the ST3L.

The pressure drop of the ST3L is tremendously higher than for the STE. This can be explained by the more complex shape of the three-lobed cross-section where the flow is constrained to go inside the lobes. Besides, the swirling flow in the three-lobed tube is more intense thus the shear stress on the wall is also greater thus causing more energetic loss. Ultimately the geometrical transitions parts between the three-lobed and the circular cross-section could also cause significant

pressure loss as the drop of the swirl intensity in phase 2 suggests on Figure 12.

5.2.3. Heat transfer and PEC

The evolution of the heat transfer enhancement for the STE and ST3L is shown on Figure 15.

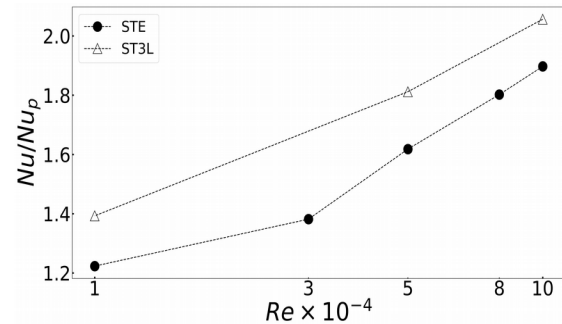


Fig.15: Evolution of Nu/Nu_p for the STE and the ST3L with Re .

It can be noticed that the heat transfer is more enhanced with the ST3L than with the STE. This is because a greater portion of the flow undergoes a swirling motion thus not only more heat is transferred from the wall of the tube to the flow in its vicinity but also more heat is transferred from the flow close to the wall to the core flow. In addition, as the wetted area of the ST3L is lower than the wetted area of the circular cross-section tube ($A_{ST3L}=225\text{mm}^2$ and $A=314\text{mm}^2$) the heat transfer enhancement is solely due to the flow structure modification and not to an increase of the heat transfer surface. The increased level of turbulence should also play a major role in this increased heat transfer.

Although heat transfer is greatly enhanced with the ST3L, pressure drop is also really high and the energetic performance of this tube geometry should be assessed. The evolution of the PEC for the STE and the ST3L can be seen on Figure 16 and it can be concluded that both technologies have almost the same energetic performances. However, for the lowest Reynolds number the PEC of the three-lobed tube is below 1 which means that the pressure drop penalty overbalances the heat transfer enhancement. Nevertheless, for higher Reynolds numbers the PEC is greater than 1. Both technologies enable to have good energetic performances but the swirling flow generated by the ST3L is more intense and can last over a longer distance than in the STE.

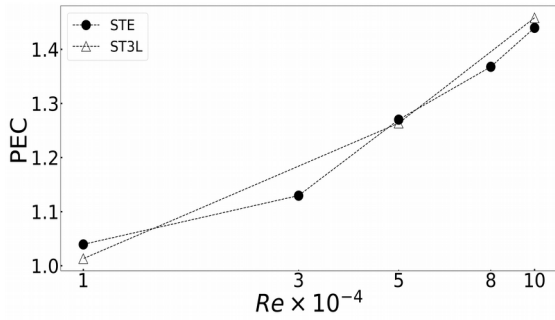


Fig.16: Evolution of the PEC for the STE and the ST3L with the Reynolds number.

CONCLUSION

The present study pursues the work of Indurain et al. [22] and further investigates the influence of the aspect ratio of a short-length twisted tube with an elliptic cross-section (STE) on heat transfer and pressure drop generated by a developing and decaying swirling flow. The effects of the modification of the cross-section from an ellipse to a three-lobed (ST3L) on the generated swirling flow, heat transfer and pressure drop are also investigated. The main conclusions of the present study are as follow:

- The STE is effective at creating a swirling flow but its intensity greatly depends on the aspect ratio.

- The lower the aspect ratio and the longer the decay of the swirling flow in the tube downstream with a circular cross-section.

- The ST3L can generate a more intense swirling flow than the STE with $c=0.6$.

- Tremendous pressure drop is generated with the ST3L and even if its PEC is almost the same as with the STE, this can be really detrimental for some applications.

- The maximum swirl intensity with the ST3L is reached early in phase 1. Therefore, the length of the ST3L might be shortened in order to keep an intense swirling flow while diminishing the pressure drop.

Furthermore, it was also emphasized that the geometrical transitions parts between the non-circular and the circular cross-sections cause a discontinuity in the evolution of the swirl intensity and thus might also cause significant singular pressure drop. Hence, these transitions parts have to be modified in order to reduce the energetic loss.

Acknowledgment

The authors would like to thank the financial support of the Association National Recherche Technologie (ANRT) through the CIFRE grant number 2017/1437.

References

- [1] A. Hasanpour, M. Farhadi, K.Sedighi, A review study on twisted tape inserts on turbulent flow heat exchangers: The overall enhancement ratio criteria, *International Communications in Heat and Mass Transfer*, Volume 55, 2014, Pages 53-62
- [2] M. Bahiraei, N. Mazaheri and S.Hassanzamani, Efficacy of a new graphene-platinum nanofluid in tubes fitted with single and twin twisted tapes regarding counter and co-swirling flows for efficient use of energy, *International Journal of Mechanical Sciences*, Volume 150, 2019, Pages 290-303
- [3] M. Bahiraei, N. Mazaheri and F. Aliee, Second law analysis of a hybrid nanofluid in tubes equipped with double twisted tape inserts, *Powder Technology*, Volume 345, 2019, Pages 692-703
- [4] S. Zhang, L. Lu, C. Dong, S. H. Cha, Performance evaluation of a double-pipe heat exchanger fitted with self-rotating twisted tapes, *Applied Thermal Engineering*, Volume 158, 2019, 113770
- [5] P. Eiamsa-ard, N. Piriyaunroj, C. Thianpong, S.Eiamsa-ard, A case study on thermal performance assessment of a heat exchanger tube equipped with regularly-spaced twisted tapes as swirl generators, *Case Studies in Thermal Engineering*, Volume 3, 2014, Pages 86-102
- [6] S. Eiamsa-ard, C. Thianpong, P. Eiamsa-ard, P. Promvong Convective heat transfer in a circular tube with short-length twisted tape insert, *International Communications in Heat and Mass Transfer*, Volume 36, Issue 4, 2009, Pages 365-371
- [7] A. Nandagawli, V. Kriplani, P. Walke, Effect of Swirl Producing Turbine Type Inserts on Heat Transfer Enhancement using Passive Method: A Review, *International Journal for Scientific Research & Development*, Volume 3, Issue 12, 2016, Pages 472-474
- [8] B. Shome, M. Jensen, Review on laminar flow and heat transfer in internally finned tubes, *Journal of Enhanced Heat Transfer*, Volume 24, Issue 1-6, 2017, Pages 339-356
- [9] K. Mohapatra, R. Mallick, D. Das and S. Pothal, Internal Finned Tube Heat Transfer Equipment for Higher Performance, *International Journal of Advanced Mechanical Engineering*, Volume 8, 2018, Pages 199-204

- 1
2
3
4
5
6
7
8
9
10
11
12
13
14
15
16
17
18
19
20
21
22
23
24
25
26
27
28
29
30
31
32
33
34
35
36
37
38
39
40
41
42
43
44
45
46
47
48
49
50
51
52
53
54
55
56
57
58
59
60
61
62
63
64
65
- [10] M. Van Goethem and E. Jelsma, Numerical and experimental study of enhanced heat transfer and pressure drop for high temperature applications, *Chemical Engineering Research and Design*, Volume 92, 2014, Pages 663-671
- [11] A. Rocha, A. Bannwart and M. Ganzarolli, Numerical and experimental study of an axially induced swirling pipe flow, *International Journal of Heat and Fluid Flow*, Volume 53, 2015, Pages 81-90
- [12] M. Ahmadvand, A. Najafi and S. Shahidinejad, An experimental study and CFD analysis towards heat transfer and fluid flow characteristics of decaying swirl pipe flow generated by axial vanes, *Meccanica*, Volume 45, 2010, Pages 111-129
- [13] T. Bali and B. Saraç, Experimental investigation of decaying swirl flow through a circular pipe for binary combination of vortex generators, *International communication in Heat and Mass Transfer*, Volume 53, 2014, Pages 174-179
- [14] K. Navickaitė, L. Cattani, C. Bahl and K. Engelbrecht, Elliptical double corrugated tubes for enhanced heat transfer, *International Journal of Heat and Mass Transfer*, Volume 128, 2018, Pages 363-377
- [15] C. Wu, C. Chen, Y. Yang and K. Huang, Numerical simulation of turbulent flow forced convection in a twisted elliptical tube, Volume 132, 2018, Pages 199-208
- [16] F. Xin, Z. Liu, N. Zheng, P. Liu and W. Liu, Numerical study on flow characteristics and heat transfer enhancement of oscillatory flow in a spirally corrugated tube, *International Journal of Heat and Mass Transfer*, Volume 127, 2018, Pages 402-413
- [17] X. Tan, D. Zhu, G. Zhou and L. Zeng, Experimental and numerical study of convective heat transfer and fluid flow in twisted oval tubes, *International Journal of Heat and Mass Transfer*, Volume 55, 2012, Pages 4701-4710
- [18] M Omid, M Farhadi, M Jafari, Numerical study on the effect of using spiral tube with lobed cross section in double-pipe heat exchangers, *Journal of Thermal Analysis and Calorimetry*, Volume 134, Issue 3, 2018, Pages 2397-2408
- [19] M Omid, M Farhadi, AAR Darzi, Numerical study of heat transfer on using lobed cross sections in helical coil heat exchangers: Effect of physical and geometrical parameters, *Energy Conversion and Management*, Volume 176, 2018, Pages 236-245
- [20] M. Jafari, S. Dabiri, M. Farhadi and K. Sedighi, Effects of a three-lobe swirl generator on the thermal and flow fields in a heat exchanging tube: An experimental and numerical approach, *Energy Conversion and Management*, Volume 148, 2017, Pages 1358-1371
- [21] J. Zhou, C. Du, S. Liu and Y. Liu, Comparison of three types of swirling generators in coarse particle pneumatic conveying using CFD-DEM simulation, *Powder Technology*, Volume 301, 2016, Pages 1309-13020
- [22] B. Indurain, F. Beaubert, D. Uystepuyst, S. Lalot and M. Couvrat, Numerical investigation of various geometries of steam cracking tubes for reduced fouling rate, *Proceedings of Heat Exchangers Fouling and Cleaning XIII*, 2019
- [23] C. Greenshield, CFD direct Ltd, OpenFOAM User Guide version 4.0, ©2011-2016 OpenFOAM Foundation Ltd
- [24] X. Tang, X. Dai and D. Zhu, Experimental and numerical investigation of convective heat transfer and fluid flow in twisted spiral tube, *International Journal of Heat and Mass Transfer*, Volume 90, 2015, Pages 523-541
- [25] E. Robertson, V. Choudhury, S. Bhushan and D. Walters, Validation of OpenFOAM numerical methods and turbulence models for incompressible bluff body flows, *Computers and Fluids*, Volume 123, 2015, Pages 122-145
- [26] P. Roache, Perspective: A Method for Uniform Reporting of Grid Refinement Studies, *Journal of Fluids Engineering*, Volume 116, 1994, Pages 405-413
- [27] M. Ali, C. Doolan and V. Wheatley, Grid convergence study for two-dimensional simulation of flow around a square cylinder at a low Reynolds number, 7th International Conference on CFD in the Minerals and Process Industries, 2009
- [28] D. Juretic, cfMesh User Guide, 2015
- [29] O. Kitoh, Experimental study of turbulent swirling flow in a straight pipe, *Journal of Fluid Mechanics*, Volume 225, 1991, Pages 445-479
- [30] W. Steenbergen and J. Voskamp, The rate of decay of swirl in turbulent pipe flow, *Flow Measurement and Instrumentation*, Volume 9, 1998, Pages 67-78
- [31] A. Najafi, S. Mousavian and A. Amini, Numerical investigations on swirl intensity decay rate for turbulent swirling flow in a fixed pipe, *International Journal of Mechanical Sciences*, Volume 53, 2011, Pages 801-811
- [32] F. Beaubert, H. Pálsson, S. Lalot, I. Choquet, H. Bauduin, Fundamental mode of freely decaying laminar swirling flows,

Applied Mathematical Modelling, Volume
40, Issues 13–14, 2016, Pages 6218-6233

- [33] R. L. Webb and E. R. G. Eckert,
Application of rough surfaces to heat
exchanger design, International Journal of
heat and Mass Transfer, Volume 15, 1972,
Pages 1647-1658

1
2
3
4
5
6
7
8
9
10
11
12
13
14
15
16
17
18
19
20
21
22
23
24
25
26
27
28
29
30
31
32
33
34
35
36
37
38
39
40
41
42
43
44
45
46
47
48
49
50
51
52
53
54
55
56
57
58
59
60
61
62
63
64
65